Plant-wide Optimal Control of an Offshore De-oiling Process Using MPC Technique

Leif Hansen * **Petar Durdevic** * **Kasper L. Jepsen** * **Zhenyu Yang** *

* *Department of Energy Technology, Aalborg University, Denmark (e-mail: lha, pdl, klj, yang@et.aau.dk).*

Abstract:
This paper investigates the optimal control solution using MPC for a typical offshore topside de-oiling process. By regarding the combination of the upstream three-phase gravity separator and the downstream de-oiling hydrocyclone set-up as one integrated *plant*, the plant-wide control problem is formulated and handled using MPC technology. The de-oiling dynamics of the hydrocyclone are estimated via system identification while the key dynamics of the considered gravity separator are modeled based on mass balance and experimental parameter estimation. The developed MPC solution is simulated and experimentally validated via a lab-scaled pilot plant. The comparison of performances of the MPC controlled system with those of a PID controlled system, which emulates the commonly deployed control solution in most current installations, shows the promising results in optimally balancing the gravity separator's (level) control and hydrocyclone's (PDR) control.

Keywords: MPC, separation process, gravity-based separator, de-oiling hydrocyclone

NOMENCLATURE

$\boldsymbol{O}_b$	Observability matrix
$\mathbf{0}_{x,y}$	Notation for zero matrix with size $x \times y$
$\boldsymbol{A}$	System matrix
$\boldsymbol{B}$	Input matrix
$\boldsymbol{C}$	Output matrix
$\boldsymbol{D}$	Feed-through matrix
$\boldsymbol{e}$	Tracking error
$\boldsymbol{Q}$	Process noise covariance matrix
$\boldsymbol{R}$	Measurement noise covariance matrix
$\boldsymbol{r}$	Reference
$\boldsymbol{S}_u$	Input matrix (prediction structure)
$\boldsymbol{S}_x$	System matrix (prediction structure)
$\boldsymbol{S}_{u1}$	Previous input matrix (prediction structure)
$\boldsymbol{u}$	Input vector
$\boldsymbol{u}_\Delta$	Incremental control
$\boldsymbol{V}$	Tracking error weighting matrix
$\boldsymbol{W}$	Control weighting matrix
$\boldsymbol{w}$	Standard normal distributed white noise
$\boldsymbol{x}$	State vector
$\boldsymbol{y}$	Output vector
h_s	Level inside the gravity separator
J	Cost function
k	Hammerstein function coefficients
n	Length of control horizon
p	Length of prediction horizon
P_{dr}	Pressure drop ratio (PDR)
Q_s	Flow rate into the gravity separator
$U_{Vo,h}$	Output from the Hammerstein function
U_{Vo}	Input to valve V_o
U_{Vu}	Input to valve V_u

Subscripts

c	Control
id	Input disturbance model
m	Measured
max	High constrain
min	Low constrain
mn	Measurement noise
o	Model used for observer design
od	Output disturbance model
p	Plant model
r	Prediction model
T	Terminal
um	Unmeasured

1. INTRODUCTION

As active oil and gas reservoirs age the water fraction in the reservoirs increase and the fluid which is received at the processing platforms contains an increased amount of water which has to be separated from the oil before the water is discharged into the oceans. The overall increase in water cut can be seen in Fig. 1, where the water to oil ratio at the year 2014 was barely 350% for the Danish sector of the North sea. This is strenuous on the water treating facilities which in some cases fail to comply with the regulations (Energistyrelsen, 2015; Miljoestyrelsen, 2010), which state a discharge limit of $30mg/l$ oil in water (OiW) concentration. One of the main challenges in the current offshore water treatment facilities is a fluctuation in the inlet flow, which has been proven to have a negative effect on the production (Husveg, 2007; Husveg et al., 2007b,a). In many cases the water treatment facilities consist of gravity separators and hydrocyclone separators, where both separation techniques take advantage of the density differences in the different phases, in most cases: water, oil, and natural gas, where this work focuses on the first two phases.

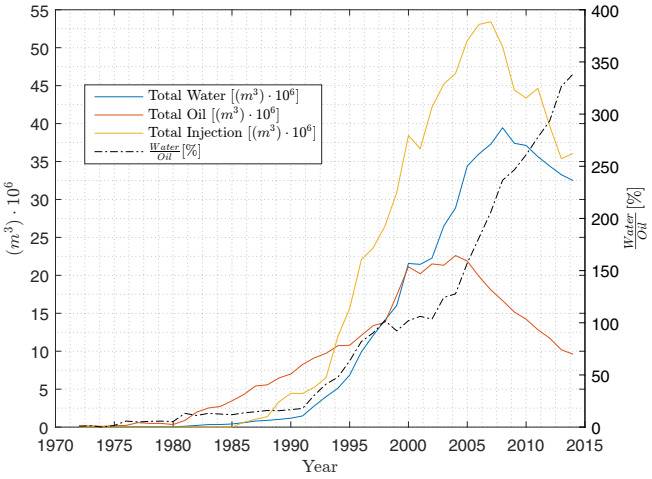

Fig. 1. Total water, oil and injection water and the increase in water/oil ratio in the Danish sector of the North Sea (Energistyrelsen, 2015).

In previous studies it was suggested that the system would benefit from an updated control structure, where the current control is in most cases based on ad-hoc tuned PID control (Yang et al., 2013). The main reason for this is that the system is physically and functionally coupled and thus the fluctuation in the inlet flow to the gravity separator can be propagated through the gravity separator to affect the hydrocyclone (Yang et al., 2014). Some previous work has investigated a robust H_∞ control solution with some promising results as stated in Durdevic (2017) and Durdevic and Yang (2018).

In this work we investigate the feasibility and potential benefits of Model Predictive Control (MPC), to handle the control problem presented in the previous works. The motivation for using MPC lie in a number of factors, such as: i) constraints to the control and process variables can be explicitly considered in the control design; ii) The predictive mechanism can help compensate some slow system dynamics; and iii) The MPC solution can facilitate on-line estimation and optimization, such that it could be applied to wider operating conditions and requirements than most "fixed" control solutions. In addition, the MPC techniques are widely applied in the industry and are more compelling for future implementation in the offshore industries.

In this work, we employed the mathematical models developed in Durdevic (2017) and Durdevic and Yang (2018), to design, test and analyse an MPC control solution. The rest of the paper is structured as follows: Section 2 describes the water treatment system, Section 3 introduces the mathematical model of the considered system, Section 4 illustrates the MPC design, Section 5 presents simulated results, Section 6 presents the experimental results, and Section 7 concludes the work.

2. CONSIDERED SYSTEM

A simplified sketch of the considered system is shown in Fig. 2. The system consists of a gravity separator and a deoiling hydrocyclone separator. The gravity separator is supplied with water, oil, and gas from the reservoir.

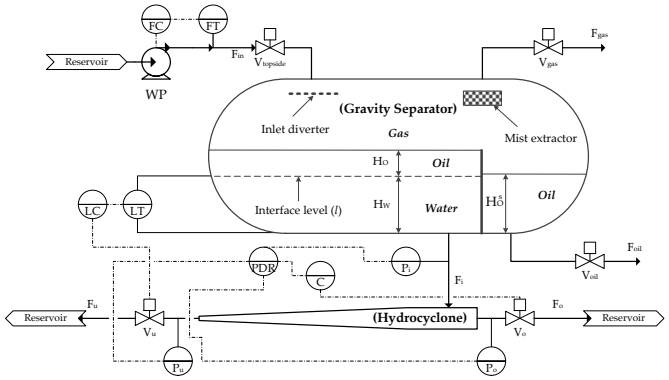

Fig. 2. Simplified diagram of the considered water treatment process, including a the three phase gravity separator and one downstream deoiling hydrocyclone separator.

The main manipulated variables of this system are the two control valves located on the hydrocyclone separator, the underflow valve V_u and the overflow valve V_o. The controlled variables of this system is the level and the Pressure Drop Ratio (PDR). Commonly this type of system is controlled using two individual control loops. (Belaidi and Thew, 2003; Sayda and Taylor, 2007; Thew, 2000; Meldrum et al., 1987).

One example of such a systems performance is shown in Durdevic et al. (2017), here it can be seen how the system during fluctuating flow, referred to as slugging, has poor performance wrt. the PDR, the level, and the valve actuation. The slugging affects the level as it introduces large amounts of liquid with an fluctuating intensity into the gravity separator, the level controller which aims at tracking the level reference actuates V_u aggressively and thus consequently affects the PDR with large fluctuations, even with PDR responses beyond the safe PDR boundary.

2.1 Pilot-Plant

All experiments are carried out in this paper, are done on a scaled pilot plant of the offshore oil and gas separation system, designed and built at Aalborg University Esbjerg (Durdevic, 2017). The plant consists of a reservoir, pipeline, riser, gravity separator, and hydrocyclone, all connected together to emulate a offshore scenario. The pipelines leading to the gravity separator are 2 inch pipes, which operate at a maximal flow of 1 l/s and pressure of 10 bars. The hydrocyclone is an industrial 35 mm VOR-TOIL hydrocyclone liner. The level of the liquid inside the gravity separator is measured using a delta pressure level transmitter and the PDR is calculated based on three pressure measurements on the hydrocyclone, i.e., inlet pressure P_i, underflow pressure P_u and the overflow pressure P_o. The reservoir is emulate by a set of tanks, and the flows are controlled using flow measurements as feedback. The system is controlled through Mathwork's Matlab Simulink Real Time platform which is interfaced to the sensors and actuators through a National Instruments Data Acquisition card.

3. MATHEMATICAL MODELS

All linear models in this paper are represented in standard state space form:

$$\dot{\boldsymbol{x}} = \boldsymbol{A}\boldsymbol{x} + \boldsymbol{B}\boldsymbol{u} \tag{1a}$$
$$\boldsymbol{y} = \boldsymbol{C}\boldsymbol{x} + \boldsymbol{D}\boldsymbol{u} \tag{1b}$$

Where all vectors and matrices in a model share a common subscript.

3.1 Linear Plant-Model

The model of the pilot-plant in Durdevic and Yang (2018) will serve as a basis for the linear plant-model in this work.

To improve the model for use in MPC design it is extended in the the following ways:

- The gravity separator inflow Q_s is added as an input.
- The changing rate of P_{dr} ($\dot{P}_{dr}$) is added as an output.

The added input is important for a good prediction, while the added output is intended for use in the cost-function, both extensions will be seen as unmeasured.

The base model and the extensions are combined to complete the linear plant-model. The vectors $\boldsymbol{u}_p$ and $\boldsymbol{y}_p$ describes the difference between the input and output and the equilibrium point.

$$\boldsymbol{u}_p = \begin{bmatrix} U_{Vu} \\ U_{Vo} \\ Q_s \end{bmatrix} - \begin{bmatrix} 0.4168 \\ 0.1657 \\ 0.4 \end{bmatrix} \tag{2a}$$

$$\boldsymbol{y}_p = \begin{bmatrix} h_s \\ P_{dr} \\ \dot{P}_{dr} \end{bmatrix} - \begin{bmatrix} 0.15 \\ 2 \\ 0 \end{bmatrix} \tag{2b}$$

Of the five states in $\boldsymbol{x}_b$ the first is equal to $h_s - 0.15$, while the remaining four stem from black-box modeling of the dynamic relationship between the valves and the PDR. The system matrices for this model are:

$$\boldsymbol{A}_p = \begin{bmatrix} -1.23\,\mathrm{e}^{-5} & 0 & 0 & 0 & 0 \\ 0 & -0.9745 & -0.7606 & 0 & 0 \\ 0 & 1 & 0 & 0 & 0 \\ 0 & 0 & 0 & -0.9316 & -0.6540 \\ 0 & 0 & 0 & 1 & 0 \end{bmatrix} \tag{3a}$$

$$\boldsymbol{B}_p = \begin{bmatrix} -1.369\,\mathrm{e}^{-3} & 0 & 1.7\,\mathrm{e}^{-3} \\ -1 & 0 & 0 \\ 0 & 0 & 0 \\ 0 & 1 & 0 \\ 0 & 0 & 0 \end{bmatrix} \tag{3b}$$

$$\boldsymbol{C}_p = \begin{bmatrix} 1 & 0 & 0 & 0 & 0 \\ 0 & 0 & 2.7204 & 0 & 1.6872 \\ 0 & 2.7204 & 0 & 1.6872 & 0 \end{bmatrix} \tag{3c}$$

$$\boldsymbol{D}_p = \boldsymbol{0}_{3,3} \tag{3d}$$

3.2 Hammerstein Plant-Model

The steady state relationship between U_{Vo} and P_{dr} is highly nonlinear, as a results the linear model has poor accuracy when, the system is operating far from the model's equilibrium point. An alternative plant-model is made with this;

$$U_{Vo,h} = arctan(U_{Vo}\ k_1)\ k_2 \tag{4}$$

Hammerstein extension added, to improve the accuracy. The constants k_1 and k_2 are experimentally determined to: $k_1 = 6$ and $k_2 \approx 0.212$. The input vector to the dynamic part of the Hammerstein model is

$$\boldsymbol{u}_{p,h} = \begin{bmatrix} U_{Vu} \\ U_{Vo,h} \\ Q_s \end{bmatrix} - \begin{bmatrix} 0.4168 \\ 0.1657 \\ 0.4 \end{bmatrix} \tag{5}$$

while the dynamic part itself is equal to the linear model.

4. MPC DESIGN

The linear plant model is augmented with an input disturbance, an output disturbance, and a measurement noise models. The augmented system is reformulated into two augmented models, one is used to design an observer for the augmented system and the other is the prediction model for the MPC solutions. As the dynamic part of the Hammerstein model is equal to the linear model, the same observer and prediction model is part of both MPC solutions.

4.1 MPC Augmented Models

As $\boldsymbol{u}_p$ contains both the controllable inputs and unmeasured input disturbance, $\boldsymbol{u}_c$ and $\boldsymbol{u}_{um}$ are defined as

$$\boldsymbol{u}_c = \boldsymbol{u}_p[1,2], \qquad \boldsymbol{u}_{um} = \boldsymbol{u}_p[3] = \boldsymbol{y}_{id} \tag{6}$$

Where $\boldsymbol{y}_{id}$ is the output from the input disturbance model, and the notation $\boldsymbol{u}_p[1,2]$ is the first and second element of $\boldsymbol{u}_p$. To make assumptions about the behavior of $\boldsymbol{u}_{um}$ the input disturbance model is modeled as

$$\boldsymbol{A}_{id} = \boldsymbol{0}_{1,1}, \qquad \boldsymbol{B}_{id} = [\,0.0588\,] \tag{7a}$$
$$\boldsymbol{C}_{id} = \boldsymbol{I}_{1,1}, \qquad \boldsymbol{D}_{id} = \boldsymbol{0}_{1,1} \tag{7b}$$

The main assumption is that $\boldsymbol{u}_{um}$ is only slowly changing (compared to the bandwidth of the observer) and can be seen as constant in the prediction horizon.

As $\boldsymbol{y}_p$ contains both the measured and unmeasured outputs, $\boldsymbol{y}_m$ and $\boldsymbol{y}_{um}$ are modeled as

$$\boldsymbol{y}_m = \boldsymbol{y}_p[1,2] + \boldsymbol{y}_{od} + \boldsymbol{y}_{mn}, \qquad \boldsymbol{y}_{um} = \boldsymbol{y}_p[3] \tag{8}$$

Where $\boldsymbol{y}_{od}$ and $\boldsymbol{y}_{mn}$ are outputs of the output disturbance model and the measurement noise model respectively.

To compensate for model errors the output disturbance model

$$\boldsymbol{A}_{od} = \boldsymbol{0}_{1,1}, \qquad \boldsymbol{B}_{od} = [\,1\,] \tag{9a}$$
$$\boldsymbol{C}_{od} = \begin{bmatrix} 0 \\ 1 \end{bmatrix}, \qquad \boldsymbol{D}_{od} = \boldsymbol{0}_{2,2} \tag{9b}$$

adds a bias state to the plant-model's prediction of $\boldsymbol{y}_p[2]$, as long as the combined system is still observable, this will compensate for steady state errors in the prediction of the PDR.

The measurement noises are assumed to follow white zero-mean normal distributions with standard deviations 1 and 35, respectively, The measurement noise model is therefore

$$\boldsymbol{D}_{mn} = \begin{bmatrix} 1 & 0 \\ 0 & 35 \end{bmatrix} \tag{10}$$

The combination of the defined models into an augmented model relevant for observer design (one that don't have the unmeasured output) is:

$$\boldsymbol{u}_o = \begin{bmatrix} \boldsymbol{u}_c \\ \boldsymbol{u}_{id} \\ \boldsymbol{u}_{od} \\ \boldsymbol{u}_{mn} \end{bmatrix} + \boldsymbol{w}, \quad \boldsymbol{x}_o = \begin{bmatrix} \boldsymbol{x}_p \\ \boldsymbol{x}_{id} \\ \boldsymbol{x}_{od} \end{bmatrix}, \quad \boldsymbol{y}_o = \boldsymbol{y}_m \tag{11a}$$

$$\boldsymbol{A}_o = \begin{bmatrix} \boldsymbol{A}_p & \boldsymbol{B}_p[1..5;3]\boldsymbol{C}_{id} & \boldsymbol{0}_{5,1} \\ \boldsymbol{0}_{1,5} & \boldsymbol{A}_{id} & \boldsymbol{0}_{1,1} \\ \boldsymbol{0}_{1,5} & \boldsymbol{0}_{1,1} & \boldsymbol{A}_{od} \end{bmatrix} \tag{11b}$$

$$\boldsymbol{B}_o = \begin{bmatrix} \boldsymbol{B}_p[1..5;1,2] & \boldsymbol{B}_p[1..5;3]\boldsymbol{D}_{id} & \boldsymbol{0}_{5,2} & \boldsymbol{0}_{5,1} \\ \boldsymbol{0}_{1,2} & \boldsymbol{B}_{id} & \boldsymbol{0}_{1,2} & \boldsymbol{0}_{1,1} \\ \boldsymbol{0}_{1,2} & \boldsymbol{0}_{1,1} & \boldsymbol{B}_{od} & \boldsymbol{0}_{1,1} \end{bmatrix} \tag{11c}$$

$$\boldsymbol{C}_o = [\, \boldsymbol{C}_p[1,2;1..5] \;\; \boldsymbol{D}_p[1,2;3]\boldsymbol{C}_{id} \;\; \boldsymbol{C}_{od} \,] \tag{11d}$$

$$\boldsymbol{D}_o = [\, \boldsymbol{D}_p[1,2;1,2] \;\; \boldsymbol{D}_p[1,2;3]\boldsymbol{D}_{id} \;\; \boldsymbol{D}_{od} \;\; \boldsymbol{D}_{mn} \,] \tag{11e}$$

Where the notation $\boldsymbol{B}_p[1..5;1,2]$ represents all 5 rows and the first and second column of $\boldsymbol{B}_p$. In order to insure observability it is confirmed that the observability matrix,

$$\boldsymbol{O}_b = \begin{bmatrix} \boldsymbol{C}_o \\ \boldsymbol{C}_o\boldsymbol{A}_o \\ \cdots \\ \boldsymbol{C}_o\boldsymbol{A}_o^6 \end{bmatrix} \tag{12}$$

is full rank.

The vectors $\boldsymbol{u}_{id}$, $\boldsymbol{u}_{od}$, and $\boldsymbol{u}_{mn}$ are assumed to be zero at all times, while each element in $\boldsymbol{w}$ is assumed to be an independent white noise following a proper standard normal distribution. Under these assumptions the, state and output noises become $\boldsymbol{B}_o\boldsymbol{w}$ and $\boldsymbol{D}_o\boldsymbol{w}$, respectively. An observer is designed as a constant gain Kalman filter with its covariance matrices calculated as

$$\boldsymbol{Q} = E\left\{\boldsymbol{B}_o\boldsymbol{w}\boldsymbol{w}^T\boldsymbol{B}_o^T\right\} = \boldsymbol{B}_o\boldsymbol{B}_o^T \tag{13a}$$

$$\boldsymbol{R} = E\left\{\boldsymbol{D}_o\boldsymbol{w}\boldsymbol{w}^T\boldsymbol{D}_o^T\right\} = \boldsymbol{D}_o\boldsymbol{D}_o^T \tag{13b}$$

$$\boldsymbol{N} = E\left\{\boldsymbol{B}_o\boldsymbol{w}\boldsymbol{w}^T\boldsymbol{D}_o^T\right\} = \boldsymbol{B}_o\boldsymbol{D}_o^T \tag{13c}$$

where $E\{\cdot\}$ denotes the expected value.

As the assumed values of the inputs $\boldsymbol{u}_{id}$, $\boldsymbol{u}_{od}$, and $\boldsymbol{u}_{mn}$ are zero, but the unmeasured output $\boldsymbol{y}_{um}$ is important for the control design. Therefore the augmented model for calculating the prediction horizon is:

$$\boldsymbol{u}_r = \boldsymbol{u}_c, \qquad \boldsymbol{x}_r = \boldsymbol{x}_o, \qquad \boldsymbol{y}_r = \boldsymbol{y}_p \tag{14a}$$

$$\boldsymbol{A}_r = \boldsymbol{A}_o \tag{14b}$$

$$\boldsymbol{B}_r = \boldsymbol{B}_p[1..5;1,2] \tag{14c}$$

$$\boldsymbol{C}_r = \begin{bmatrix} \boldsymbol{C}_p & \begin{bmatrix} \boldsymbol{C}_o[1..2;6,7] \\ \boldsymbol{0}_{1,2} \end{bmatrix} \end{bmatrix} \tag{14d}$$

$$\boldsymbol{D}_r = \boldsymbol{D}_p[1,3;1,2] \tag{14e}$$

4.2 MPC Parameters

A discrete version of (14) is used to calculate $\boldsymbol{S}_x$, $\boldsymbol{S}_{u1}$, and $\boldsymbol{S}_u$ in the common discrete prediction structure,

$$\begin{bmatrix} \boldsymbol{y}_r(0) \\ \cdots \\ \boldsymbol{y}_r(p) \end{bmatrix} = \boldsymbol{S}_x\boldsymbol{x}_r(0) + \boldsymbol{S}_{u1}\boldsymbol{u}_r(-1) + \boldsymbol{S}_u \begin{bmatrix} \boldsymbol{u}_\Delta(0) \\ \cdots \\ \boldsymbol{u}_\Delta(n) \end{bmatrix}, \tag{15}$$

which is used to calculate $\boldsymbol{y}_r$ for all steps in the prediction horizon. Where the notation $\boldsymbol{y}_r(m)$ is $\boldsymbol{y}_r$ at the m^{th} step. As all references are constant at the equilibrium point, the sequence of $\boldsymbol{y}_r$ describes the tracking error for each time step in the prediction horizon as a function of $\boldsymbol{x}_r(0)$, $\boldsymbol{u}_r(-1)$, and $\boldsymbol{u}_\Delta$. As $\boldsymbol{u}_r(-1)$ is equal to the previous value of $\boldsymbol{u}_c$, and $\boldsymbol{x}_r(0)$ can be approximated by the observed sates, $\hat{\boldsymbol{x}}_o$, they are assumed to be known, leveling only $\boldsymbol{u}_\Delta$ as unknown.

The controllers sampling time is 0.2 seconds to have adequate performance of the PDR control, the prediction horizon is then needed to be quite long ($p = 600$) to allow control of the much slower gravity separator level. To have sufficient smooth valve control the control horizon is selected as $n = 30$.

The optimization problems of both the linear and Hammerstein MPC controllers are

$$\begin{aligned} \underset{\boldsymbol{u}_\Delta}{\text{minimize}} \quad & J(\boldsymbol{u}_\Delta(0),..,\boldsymbol{u}_\Delta(n),\boldsymbol{u}_c(-1),\hat{\boldsymbol{x}}_o(0)) \\ \text{subject to} \quad & \boldsymbol{c}_{min} \le \boldsymbol{y}_r \le \boldsymbol{c}_{max} \\ & \boldsymbol{d}_{min} \le \boldsymbol{u}_r \le \boldsymbol{d}_{max} \end{aligned} \tag{16}$$

where only $\boldsymbol{d}_{min}$ and $\boldsymbol{d}_{max}$ are different between the two optimization problems. These optimization problems are in the controllers rewritten to standard QP problems and solved with the KWIK algorithm from Schmid and Biegler (1994) as implemented in Matlab's MPC toolbox.

The cost function J can be written as,

$$\begin{aligned} &J(\boldsymbol{u}_\Delta(0),..,\boldsymbol{u}_\Delta(n),\boldsymbol{u}_c(-1),\hat{\boldsymbol{x}}_o(0)) = \\ &\begin{bmatrix} \boldsymbol{u}_\Delta(0) \\ \cdots \\ \boldsymbol{u}_\Delta(n) \end{bmatrix}^T \begin{bmatrix} \boldsymbol{W} & & \boldsymbol{0} \\ & \ddots & \\ \boldsymbol{0} & & \boldsymbol{W} \end{bmatrix} \begin{bmatrix} \boldsymbol{u}_\Delta(0) \\ \cdots \\ \boldsymbol{u}_\Delta(n) \end{bmatrix} + \\ &\begin{bmatrix} \boldsymbol{y}_r(0) \\ \cdots \\ \boldsymbol{y}_r(p) \end{bmatrix}^T \begin{bmatrix} \boldsymbol{V} & & & \boldsymbol{0} \\ & \ddots & & \\ & & \boldsymbol{V} & \\ \boldsymbol{0} & & & \boldsymbol{V}_T \end{bmatrix} \begin{bmatrix} \boldsymbol{y}_r(0) \\ \cdots \\ \boldsymbol{y}_r(p) \end{bmatrix} \end{aligned} \tag{17}$$

where the sequence of $\boldsymbol{y}_r$ is calculated from (15), $\boldsymbol{W}$ is the control weight, $\boldsymbol{V}$ is the tracking error weight, and $\boldsymbol{V}_T$ is the terminal tracking error weight.

The weights are experimentally selected as:

$$\boldsymbol{W} = \begin{bmatrix} 4.5 & 0 \\ 0 & 0 \end{bmatrix} \tag{18}$$

$$\boldsymbol{V} = \begin{bmatrix} 1\,\mathrm{e}^{-2} & 0 & 0 \\ 0 & 1.5 & 0 \\ 0 & 0 & 5 \end{bmatrix}, \qquad \boldsymbol{V}_T = \begin{bmatrix} 10 & 0 & 0 \\ 0 & 1.5 & 0 \\ 0 & 0 & 5 \end{bmatrix} \tag{19}$$

The design idea for $\boldsymbol{W}$ is to penalize movement of V_u in order to ensure a near constant flow between the gravity separator and the hydrocyclone.

$\boldsymbol{V}$ is designed to keep a low tracking error for P_{dr} and $\dot{P}_{dr}$ and allow the gravity separator volume to be used as a physical damping buffer of fluctuations of Q_s. $\boldsymbol{V}_T$ is used at the final step to ensure the tracking error for the level can reach zero within the prediction horizon, under the assumption that Q_s is constant.

The constraints of the actual level is selected as: $0.1m \le h_s \le 0.2m$, while no constraints are defined for P_{dr} and $\dot{P}_{dr}$. This gives the output constraints vectors

$$\boldsymbol{c}_{min} = \begin{bmatrix} -0.05 \\ -\infty \\ -\infty \end{bmatrix}, \qquad \boldsymbol{c}_{max} = \begin{bmatrix} 0.05 \\ \infty \\ \infty \end{bmatrix} \tag{20}$$

The constraints of the manipulated variables (opening degrees of the considered control valves) are: $0.1 \le U_{Vu} \le 1$ and $0.03 \le U_{Vo} \le 1$, which for the linear controller gives the input constraints

$$\boldsymbol{d}_{min} = \begin{bmatrix} -0.3168 \\ -0.1357 \end{bmatrix}, \qquad \boldsymbol{d}_{max} = \begin{bmatrix} 0.5832 \\ 0.8343 \end{bmatrix} \tag{21}$$

The controllable inputs in the dynamic part of the Hammerstein model are U_{Vu} and $U_{Vo,h}$, the constraints for $U_{Vo,h}$ are calculated with the constraints of U_{Vo} and the Hammerstein function (4) to: $0.038 \leq U_{Vo,h} \leq 0.3$. The input constraints for the Hammerstein controller then become:

$$\boldsymbol{d}_{min,h} = \begin{bmatrix} -0.3168 \\ -0.1280 \end{bmatrix}, \qquad \boldsymbol{d}_{max,h} = \begin{bmatrix} 0.5832 \\ 0.1320 \end{bmatrix} \tag{22}$$

The control sequence from the Hammerstein MPC controller are U_{Vu} and $U_{Vo,h}$. In order to find U_{Vo} the inverse Hammerstein function

$$U_{Vo} = tan\left(\frac{U_{Vo,h}}{k_2}\right)/k_1 \tag{23}$$

is used.

5. SIMULATION STUDIES

The simulated performance of the two designed MPC controllers are investigated. The linear controller is simulated against both the linear plant model and the Hammerstein extended plant model, while the Hammerstein controller is only simulated against the latter. All simulations are made with a fixed-step ODE solver (RK4) with a step size equal to the pilot-plant's sample rate of 0.01 seconds. To emulate a relevant noise, each of the simulated measured outputs is added a random number from a zero mean normal distribution with variance equal to the sample variance of steady state measurements from the pilot-plant. ZOH is used to downsample to the MPC sample rate, while the output from the controllers are kept constant between MPC steps.

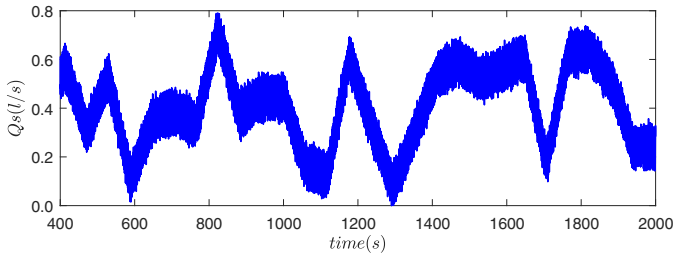

Fig. 3. Unmeasured input disturbance used in both simulations and experiments

The input disturbance signal chosen to be used in both simulations and experiments is a variation of part of the disturbance signal from the *severe operation* scenario in Durdevic (2017), made to emulate severe offshore conditions. The only modification of the signal is that it is slowed down by a factor of 0.7 to increase the severity of the derivations from equilibrium. In Fig. 3 a measurement of this signal form one of the experiments is seen. All simulations have constant references of $0.15m$ for the level and of 2 for the PDR.

Fig. 4 shows the simulated performance of the linear MPC against the linear model. In this simulation the controller can keep the PDR on the reference value as long as the level is not close to its constrains. There is only a slight

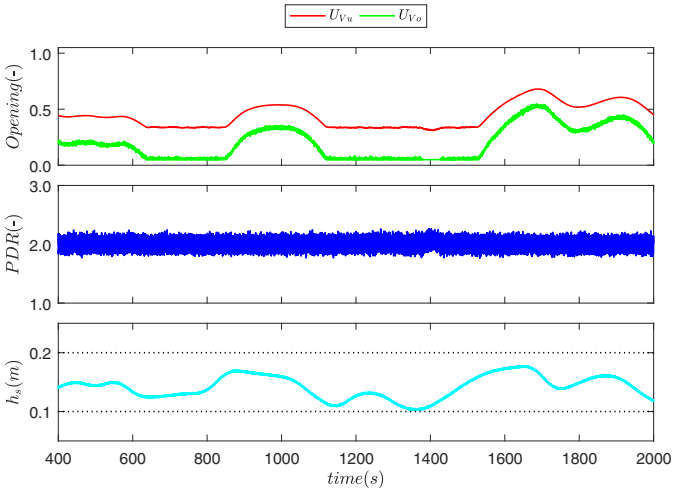

Fig. 4. Performance of the linear MPC against the linear model

variation in PDR at $time \approx 1400s$. It can also be seen that during periods with low inflow, U_{Vo} reaches its lower constraint, while during periods with high inflow both valves operate inside their constrains.

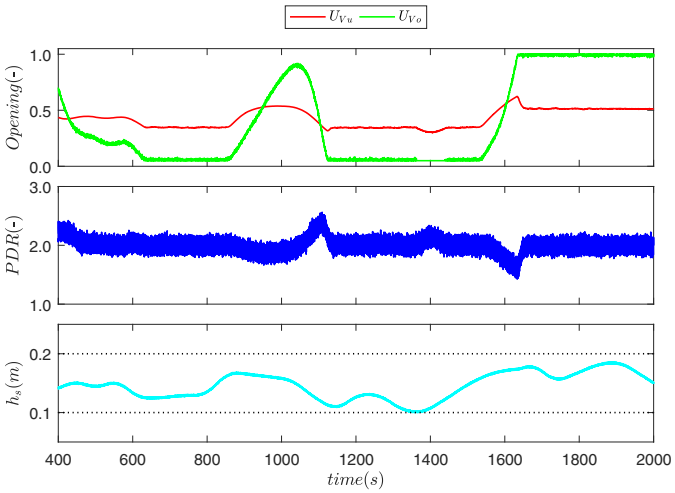

Fig. 5. Performance of the linear MPC against the Hammerstein model

The difference in the linear MPC performance, caused by the Hammertein plamt-model, can been seen by compraing Fig. 4 and Fig. 5. In the new simulation the PDR deviates from its reference while the valves are moving and only in steady state it settles at the reference. After this model extension U_{Vo} also reaches its high constraint under periods with high inflow.

Fig. 6 shows the Hammerstein MPC controller simulated with the Hammerstein model, U_{Vo} still reaches its constraints in both directions but the PDR performance is similar to that of the linear controller in Fig. 4. The average level is higher in this simulation in comparison to the previous simulations as U_{Vu} is more limited when using this controller as U_{Vo} reaches its high constraint, resulting in a reduced PDR control performance at $time \approx 1900s$ to keep the level within its high constraint.

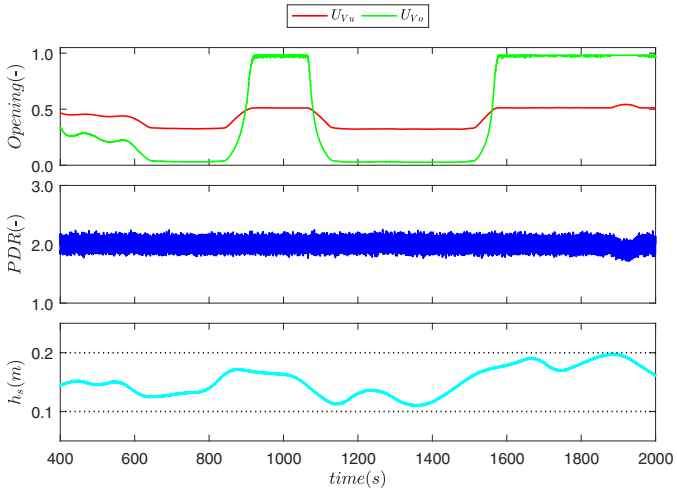

Fig. 6. Performance of the Hammerstein MPC against the Hammerstein model

6. EXPERIMENTAL TESTING

The PID controller and the H_∞ robust controller designed in Durdevic (2017) are compared with the two MPC controllers using the pilot-plant. All experiments have the same input disturbance and references as the simulations.

The controllers are all implemented directly in Mathworks Matlab Simulink Real Time platform and sample rate transitions for the MPC controllers are handled in the same way as in simulations.

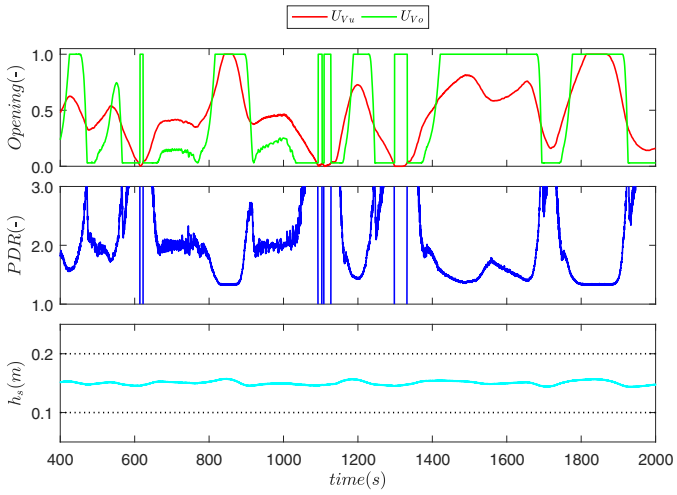

Fig. 7. Experimental performance of the PID controller

Fig. 7 shows that the PID-controller can not maintain tracking of the PDR reference due to valve saturation, which could lead to reduced efficiency of the hydrocyclone (Meldrum et al., 1987; Thew, 2000).

The robust controller in Fig. 8 keeps a relatively steady PDR, but allows the gravity separator level to reach a high level potentially compromising the gravity separator's efficiency.

The linear MPC controller illustrated in Fig. 9 keeps a level closer to the reference than the robust controller, but at the tradeoff of the PDR variations. The main benefit of this controller is the use of constraints to keep the level

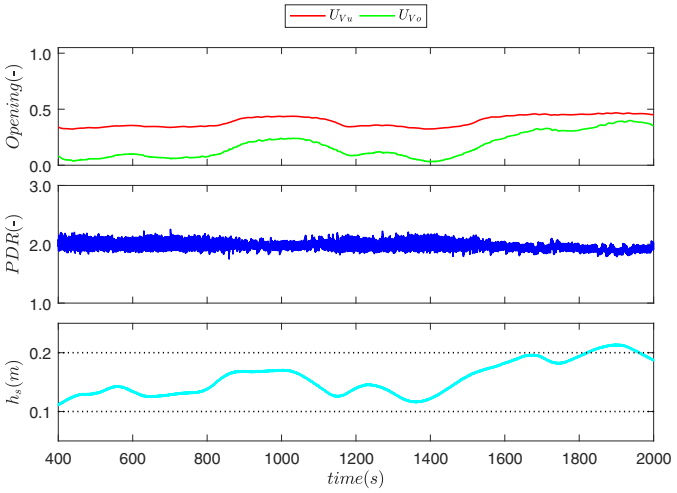

Fig. 8. Experimental performance of the H_∞ controller

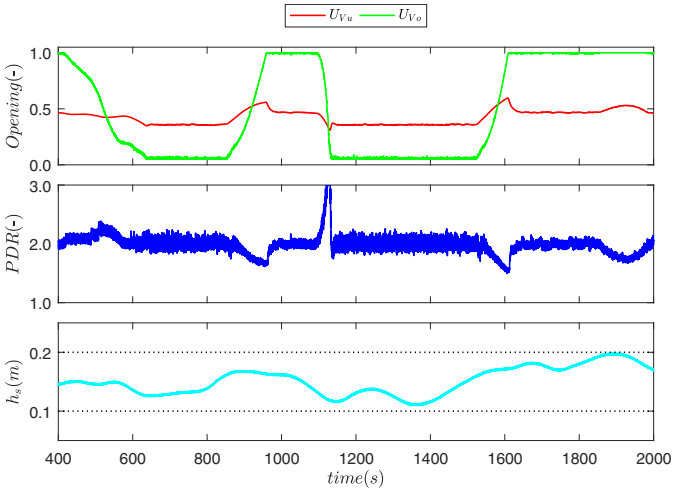

Fig. 9. Experimental performance of the linear MPC

within an interval. The deviation from reference value of the PDR is highest when the valves are moving, while the PDR reaches the reference value when the valves are steady. This could be an indicator that the controller is highly dependent on the integral action from the output disturbance model to counteract model errors in the linear plant model. The only exception to this observation is near the end of the experiment (at $time \approx 1900s$) where the deviation in PDR is caused by the level reaching its constraint. It is also evident that the linear MPC controller operates the valves further from the equilibrium point of the linear model than the robust controller, this could be the reason for this experiment's PDR variations compared to the controllers simulated performance shown in Fig. 4.

Comparing the experiment in Fig. 9 with the simulations in Fig. 4 and Fig. 5 it can be seen that the Hammerstein model better describes the pilot-plant but still leaves room for improvement.

Compared to the linear MPC controller the results from the Hammerstein MPC controller in Fig. 10 show a faster response of U_{Vo} and less deviation from reference of the PDR. The level has in general close to the same response as in Fig. 9, but it is a little higher throughout the experiment

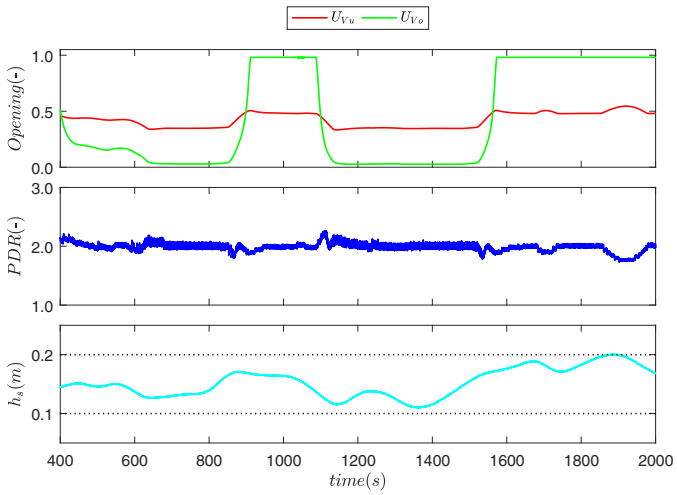

Fig. 10. Experimental performance of the Hammerstein MPC

and reaches its constraint twice (at $time \approx 1700s$ and $time \approx 1900s$) instead of only once.

7. CONCLUSIONS AND FUTURE WORKS

The performance of the two MPC control solutions has been compared to the PID and H_∞ controllers. From our experimental results we see a clear improvement in the system performance when using the H_∞ control solution in comparison to the PID control solution, as the PDR and the valves no longer saturate and the PDR remains stable in a safe region around the PDR reference of 2. The tradeoff is on the level, which fluctuates more compared to the PID control solution and dose not stay within the constraints of $0.1m$ to $0.2m$.

Applying the MPC solution enable for the addition of constraints, which, in experimental results with both the MPC solutions, allows the level to be maintained within the constraints of $0.1m$ to $0.2m$. Of the two MPC solutions, only the Hammerstein MPC solution is able to keep the PDR around the reference of 2.

In this paper, we show that by applying an MPC solution the gravity separator volume can be used as a buffer for the inflow and keeps the level within the constraints under more severe conditions than the compared H_∞ control solution.

As the measurement of h_s come close to violating its high constraint in Fig 9 and Fig 10 any non experimental implementation of the MPC controllers should include slack variables to prevent infeasibility.

It is shown that the used linear model isn't sufficient for good PDR tracking, and even the suggested Hammerstein model leaves room for improvements. Future work should therefore include an improved model.

The fast response of the hydrocyclone subsystem and slow response of gravity separator subsystem are handled with a high sampling rate and a long prediction horizon, a different solution will be preferred in future work to reduce computational load.

ACKNOWLEDGEMENTS

The authors thank the support from the DTU-DHRTC and AAU joint project - Smart Water Management. Thanks also go to DTU colleagues: E. Bek-Pedersen, T. M. Jørgensen and M. Lind, AAU colleagues: M. Bram, S. Pedersen, D.S. Hansen and S. Jespersen for many valuable discussions and technical support.

REFERENCES

Belaidi, A. and Thew, M. (2003). The effect of oil and gas content on the controllability and separation in a de-oiling hydrocyclone. *Chemical Engineering Research and Design*, 81(3), 305–314.

Durdevic, P. (2017). *Real-Time Monitoring and Robust Control of Offshore De-oiling Processes*. Phd thesis, Aalborg University.

Durdevic, P., Pedersen, S., and yang, Z. (2017). Operational performance of offshore de-oiling hydrocyclone systems. *IECON 2017 - 43rd Annual Conference of the IEEE Industrial Electronics Society*, 43, 6905 – 6910.

Durdevic, P. and Yang, Z. (2018). Application of h robust control on a scaled offshore oil and gas de-oiling facility. *Energies*, Manuscript under revision for Energies.

Energistyrelsen (2015). Danish production of oil, gas and water 1972-2014 (danish energy agency). URL `https://ens.dk/`. Acssessed (09-11-2016).

Husveg, T. (2007). *Operational Control of Deoiling Hydrocyclones and Cyclones for Petroleum Flow Control*. Phd thesis, University of Stavanger.

Husveg, T., Johansen, O., and Bilstad, T. (2007a). Operational control of hydrocyclones during variable produced water flow ratesfrøy case study. *SPE Production & Operations*, 22(03), 294–300.

Husveg, T., Rambeau, O., Drengstig, T., and Bilstad, T. (2007b). Performance of a deoiling hydrocyclone during variable flow rates. *Minerals Engineering*, 20(4), 368–379. doi: http://dx.doi.org/10.1016/j.mineng.2006.12.002.

Meldrum, N. et al. (1987). Hydrocyclones: A solution to produced water treatment. In *Offshore Technology Conference*. Offshore Technology Conference.

Miljoestyrelsen (2010). Status for den danske offshore-handlingsplan til udgangen af 2009. *Miljoestyrelsen*. Acssessed (01-11-2016).

Sayda, A.F. and Taylor, J.H. (2007). Modeling and control of three-phase gravilty separators in oil production facilities. In *American Control Conference, 2007. ACC'07*, 4847–4853. IEEE.

Schmid, C. and Biegler, L.T. (1994). Quadratic programming methods for reduced hessian sqp. *Computers & chemical engineering*, 18(9), 817–832.

Thew, M. (2000). Flotation— cyclones for oil/water separations.

Yang, Z., Pedersen, S., and Durdevic, P. (2014). Cleaning the produced water in offshore oil production by using plant-wide optimal control strategy. In *Oceans-St. John's, 2014*, 1–10. IEEE.

Yang, Z., Stigkær, J.P., and Løhndorf, B. (2013). Plant-wide control for better de-oiling of produced water in offshore oil & gas production. *IFAC Proceedings Volumes*, 46(20), 45–50.